FOREX Publication
Open Access | Rapid and quality publishing

International Journal of Electrical and Electronics Research (IJEER)
Research Article | Volume 14, Issue 1 | Pages 95-103 | e-ISSN: 2347-470X

Hybrid Approach to IBC Solar Cell Simulation: Coupling of Deep Neural Network and Advanced Electrical Analysis

Farouk Tounsi[1,3], Toufik Zarede[2], Hamza Lidjici[3], and Asma Benchiheb*[4,5]

[1*]*Laboratory of Electronics and New Technologies, Oum El Bouaghi University, Algeria; Email: farouk.t91@hotmail.com*
[2]*Unité de Développement des Équipements Solaires, UDES, Centre de Développement des Énergies Renouvelables, CDER, 42415, Tipaza, Algeria; Email: toufik.zarede@gmail.com*
[3]*Laboratoire des matériaux pour application et valorisation des énergies renouvelables, Université de Laghouat. Laghouat, Algérie; Email: hlidjici@yahoo.fr*
[4]*Department of Pharmacy, Faculty of Medicine, University of Salah Boubnider - Constantine 3, Constantine 25000, Algeria; Email: asmabenchiheb@yahoo.fr*
[5]*Microsystem and Instrumentation Laboratory, Electronics Department, Technology Faculty, University of frères Mentouri-Constantine 1, Constantine 25000, Algeria; Email: asmabenchiheb@yahoo.fr*

***Correspondence:** *Asma Benchiheb, Email: asmabenchiheb@yahoo.fr*

ABSTRACT- This study introduces a sophisticated computational model developed in MATLAB to simulate the performance of interdigitated back contact (IBC) solar cells under various environmental conditions. The main objective of this work is to develop and validate a neural network that can predict I_{ph} and I_o of an IBC solar cell under varying environmental conditions (temperature and irradiance). The model is based on a deep feedforward neural network comprising two hidden layers with 20 and 10 neurons, respectively. This architecture enables accurate prediction of key electrical parameters, such as photocurrent (I_{ph}) and reverse saturation current (I_o), influenced by factors like temperature and irradiance. Trained on synthetic data representing realistic fluctuations in these variables, the neural network significantly outperforms conventional experimental models in predictive accuracy. The simulation analyzes current–voltage (I–V) and power–voltage (P–V) characteristics over a voltage range of 0 to 0.85 V, incorporating temperature-dependent ideality factors to faithfully represent physical behavior. Iterative optimization strategies were implemented to address convergence issues in open-circuit voltage calculations, ensuring realistic voltage levels (approximately 0.6–0.7 V at 100 W/m²). The model demonstrates impressive performance, accurately predicting short-circuit current (I_{sc}), open-circuit voltage (V_{oc}), maximum power point (P_{max}), fill factor (FF), and overall efficiency, all validated against expected IBC cell behavior. This predictive framework provides a versatile tool for optimizing the design and performance of IBC solar cells under dynamic operating conditions.

Keywords: IBC Solar Cell, Neural Network, electrical analysis.

ARTICLE INFORMATION

Author(s): Farouk Tounsi, Toufik Zarede, Hamza Lidjici, and Asma Benchiheb;
Received: 02/09/2025; **Accepted:** 12/01/2026; **Published:** 10/03/2026;
E- ISSN: 2347-470X;
Paper Id: IJEER 0209A02;
Citation: 10.37391/ijeer.140110
Webpage-link:
https://ijeer.forexjournal.co.in/archive/volume-14/ijeer-140110.html

Publisher's Note: FOREX Publication stays neutral with regard to jurisdictional claims in Published maps and institutional affiliations.

1. INTRODUCTION

Solar energy has become a cornerstone of the global transition toward renewable energy, with photovoltaic (*PV*) technologies evolving rapidly to improve efficiency, scalability, and adaptability under diverse environmental conditions [1]. Among the advanced PV architectures, interdigitated back contact (*IBC*) solar cells have emerged as a particularly promising design. By relocating all electrical contacts to the rear surface, *IBC* cells minimize front-side shading and significantly enhance charge carrier collection efficiency, leading to high power conversion efficiencies exceeding 26% in laboratory settings [2].

Maximizing the performance potential of *IBC* solar cells requires accurate and robust modeling tools capable of capturing their complex physical behaviors [3]. Traditional modeling approaches, such as the single-diode or double-diode equivalent circuit models, provide reasonable accuracy under standard test conditions (STC: 1000 W/m^2, 25°C) [4]. However, these models often fall short when dealing with non-linearities introduced by environmental variations such as fluctuating irradiance and temperature, particularly in advanced architectures like IBC cells where interactions between the front-surface field (*FSF*) and back-surface field (*BSF*) introduce additional complexity [5]. While numerical simulation tools like PC1D and Silvaco ATLAS offer a more detailed analysis by solving semiconductor equations, they are computationally intensive and require extensive parameter calibration, limiting their practicality for rapid design iterations or broad parametric studies [6].

FOREX Publication
Open Access | Rapid and quality publishing
International Journal of Electrical and Electronics Research (IJEER)
Research Article | Volume 14, Issue 1 | Pages 95-103 | e-ISSN: 2347-470X

In parallel, the field of photovoltaic modeling has increasingly turned toward data-driven methodologies, especially machine learning (*ML*) and artificial neural networks (*ANN*), to address the limitations of conventional models [7]. Prior studies, such as those by Almonacid et al. (2016) and Karatabe et al. (2006), have demonstrated the potential of neural networks to predict *I–V* characteristics and cell efficiencies with high accuracy, even under variable environmental conditions [8-9]. More recent efforts, including the work of Procel *et al.* (2017), have extended these techniques to IBC architectures, highlighting their ability to optimize design parameters such as contact spacing and dopant activation [10]. Hybrid approaches combining physical models with deep learning architectures, including multilayer perceptrons and recurrent neural networks, have further improved predictive performance by integrating environmental inputs like temperature and irradiance [11].

Building on this momentum, the present work introduces a MATLAB-based simulation framework that leverages a deep feedforward neural network to model the performance of *IBC* solar cells. The model predicts fundamental electrical parameters specifically photocurrent (I_{ph}) and reverse saturation current (I_o) as functions of temperature and irradiance, using a physics-informed data-driven approach. Trained on enhanced synthetic datasets, the model captures non-linear interactions and environmental dependencies more effectively than conventional empirical techniques [12]. The suggested scheme allows the standard voltage sweep to be extended beyond *2 V* significantly further than the normal range of single-junction models [13], thus providing more detailed electrical characterization of such cells as *IBC* solar. It also makes use of temperature-dependent ideality factors parameters that greatly influence the accuracy of the estimation of thermal changes in the behavior of the diode, the mechanisms of recombination, and finally, the Voc, fill factor (*FF*), and conversion efficiency [14].

Besides, whilst earlier simulation research mainly performs two-dimensional *I–V* and *P–V* curves at different irradiance and temperature [15], the current study goes further by visual features that include a *3D* surface of power versus voltage and irradiance an integral, intuitive insight into the device's characteristics through the environmental conditions. Through this hybrid methodology, the proposed framework provides a flexible, precise, and scalable tool for the analysis and optimization of IBC solar cell performance, paving the way for integration with experimental data and advanced design algorithms [16].

2. STUDIED STRUCTURE AND SIMULATION PARAMETERS

The overall structure and the electrical parameters of the investigated solar cell are illustrated in *figure 1* and *table 1*, respectively. The parameters are carefully selected using the literature [17][18].

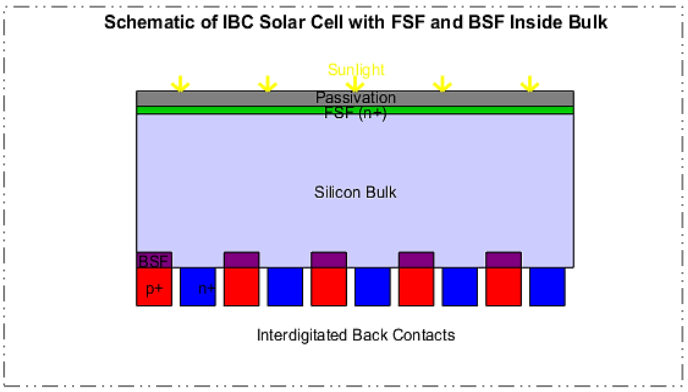

Figure 1. General structure of IBC Solae Cell

Table 1. Values of technological and physical parameters

Solar Cell Parameter	Value	Ref
Photogenerated current	$I_{ph,ref}$ = 0.05[A]	[16].
Reverse saturation current	$I_{o,ref}$=5×10^{-12}[A] (increased to improve model accuracy)	[17].
Diode ideality factor	n=1.1	[16,17].
Series resistance	R_s=0.0005 [Ω]	[18].
Shunt resistance	Rsh=2000 [Ω]	[17].

The script simulates the electrical behavior of the solar cell under the following conditions:

- Temperature range: T = [300, 305, ..., 350] [K]
- Irradiance range: G = [100, 200, ..., 1000] [W/m^2]
- Voltage sweep: V = [0, 0.01, ..., 0.85] [V]

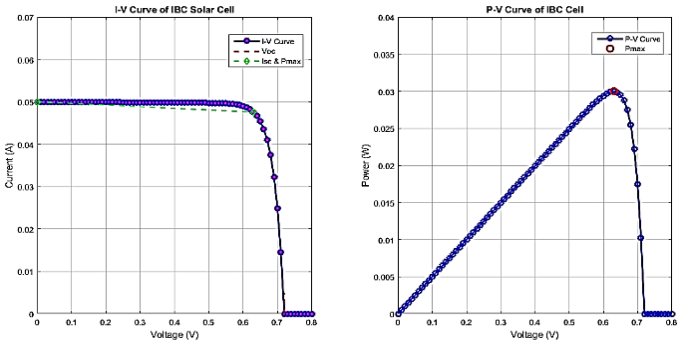

Figure 2. *I-V* and *P-V* curve of *IBC* Cell (IBC Solar Cell Metrics: Short-circuit current (I_{sc}): 0.050 A, Open-circuit voltage (V_{oc}): 0.720 *V*, Maximum power (P_{max}): 0.030 *W*, Voltage at Pmax (V_{mp}): 0.630 *V*, Current at Pmax (I_{mp}): 0.048 A, Fill factor (*FF*): 0.833, Efficiency (1000 W/m^2): 29.973%)

FOREX Publication
Open Access | Rapid and quality publishing
International Journal of Electrical and Electronics Research (IJEER)
Research Article | Volume 14, Issue 1 | Pages 95-103 | e-ISSN: 2347-470X

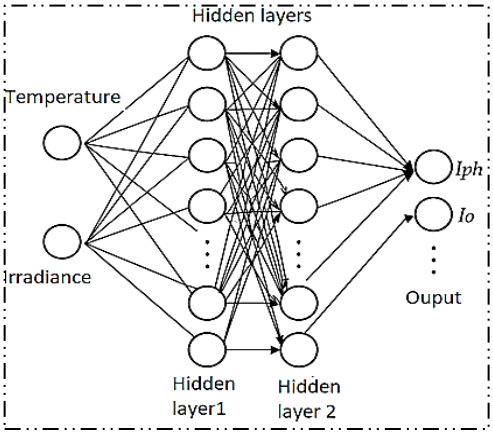

Figure 3. Neural network architecture

3. NEURAL NETWORK-BASED PREDICTION OF PHOTOGENERATED AND SATURATION CURRENTS

The model leverages a deep neural network to predict the values of the photogenerated current (I_{ph}) and the reverse saturation current (I_o) as functions of temperature (T) and irradiance (G). The training dataset is synthetically generated by varying temperature within the range of 280 K to 370 K and irradiance between 50 W/m^2 and 1200 W/m^2, ensuring coverage of a broad spectrum of realistic environmental conditions.

Expression for the photogenerated current:

$$I_{ph} = I_{ph,ref} \times \left(\frac{G}{100}\right) + \alpha_T (T-298) \quad (1)$$

Where α_T=0.0005 A/K is the temperature coefficient of the photogenerated current.

Expression for the reverse saturation current:

$$I_0 = I_{0,ref} \times exp\left(\frac{\ln(1.15)\times(T-298)}{10}\right) \times \left(\frac{G}{100}\right)^{0.5} \quad (2)$$

Where,

Symbol	Description	Value	Units
$\mathbf{I_{ph}}$	Photogenerated current	**To predict**	A
$\mathbf{I_{ph,ref}}$	Photocurrent at reference conditions	0.05	A
G	Irradiance	[100:100:1000]	$W \cdot m^{-2}$
T	Cell temperature	[300:5:350]	K
$\boldsymbol{\alpha_T}$	Temperature coefficient of photocurrent	(5.10^{-4})	$A.K^{-1}$
$\mathbf{I_0}$	Reverse saturation current	**To predict**	A
$\mathbf{I_{0,ref}}$	Reference saturation current (at 298 K, 100 W/m²)	(5.10^{-12})	A
ln(1.15)	Temperature scaling factor	—	—

The input features (T, G) and target outputs (Iph, Io) derived from these analytical expressions are used to train a deep feedforward neural network, enabling the model to generalize current predictions under diverse and dynamic operating scenarios.

4. NEURAL NETWORK CONFIGURATION AND TRAINING

A feedforward neural network architecture was implemented, comprising two hidden layers with 20 and 10 neurons, respectively:

- Hidden layers 1 and 2: Tangent sigmoid activation function (*tansig*)
- Output layer: Linear activation function (*purelin*)

The training was conducted using the Levenberg–Marquardt (trainlm) algorithm, with mean squared error (MSE) as the performance metric. The training parameters were defined as follows:

- Maximum number of epochs: 2000
- Performance goal (target MSE): 1×10^{-6}
- Data division: 70% for training, 15% for validation, and 15% for testing

After training, the network was used to predict the photogenerated current (I_{ph}) and reverse saturation current (I_o) over the predefined ranges of temperature and irradiance.

The training successfully converged, achieving the target error, as indicated in the summary panel of the MATLAB *nntraintool* interface in *figure 4*.

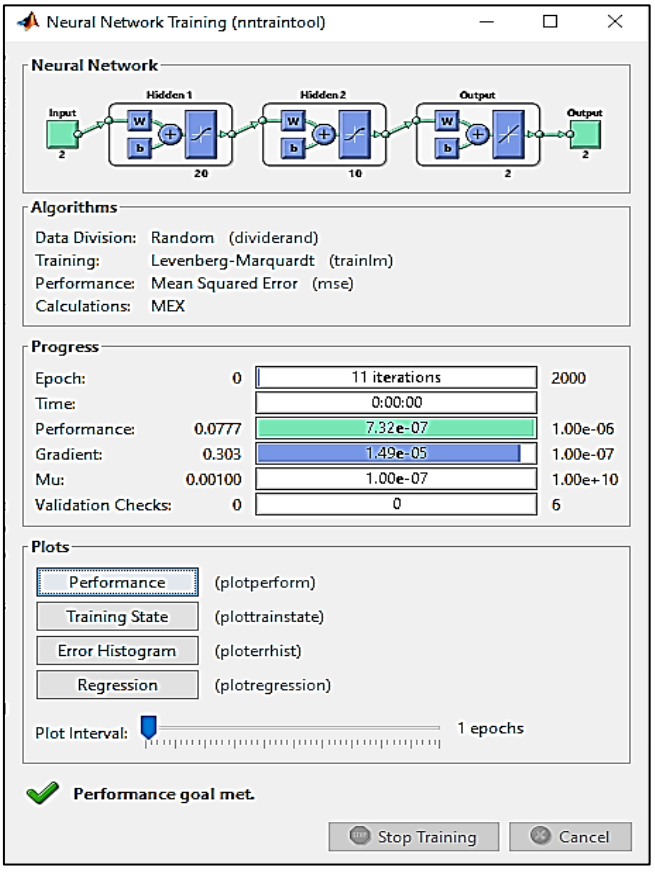

Figure 4. Neural network training

FOREX Publication
Open Access | Rapid and quality publishing
International Journal of Electrical and Electronics Research (IJEER)
Research Article | Volume 14, Issue 1 | Pages 95-103 | e-ISSN: 2347-470X

4.1. Uncertainty Quantification of Neural Network Predictions

In order to strengthen the reliability of the neural-network predictions a full uncertainty quantification stage has been added. First, the prediction error was evaluated on the test dataset by computing the RMSE and the standard deviation of the residuals. Then, an ensemble of 10 independently trained neural networks was generated in order to estimate the variability of the predictions through model diversity. For each predicted variable, the mean prediction and the ± standard deviation interval are now reported. Error bars were added to the plots (Figure 5) of *Iph*, *Io*, *Pmax*, and *Voc*. This addition significantly improves the reliability and transparency of the results and better reflects the robustness of the proposed model.

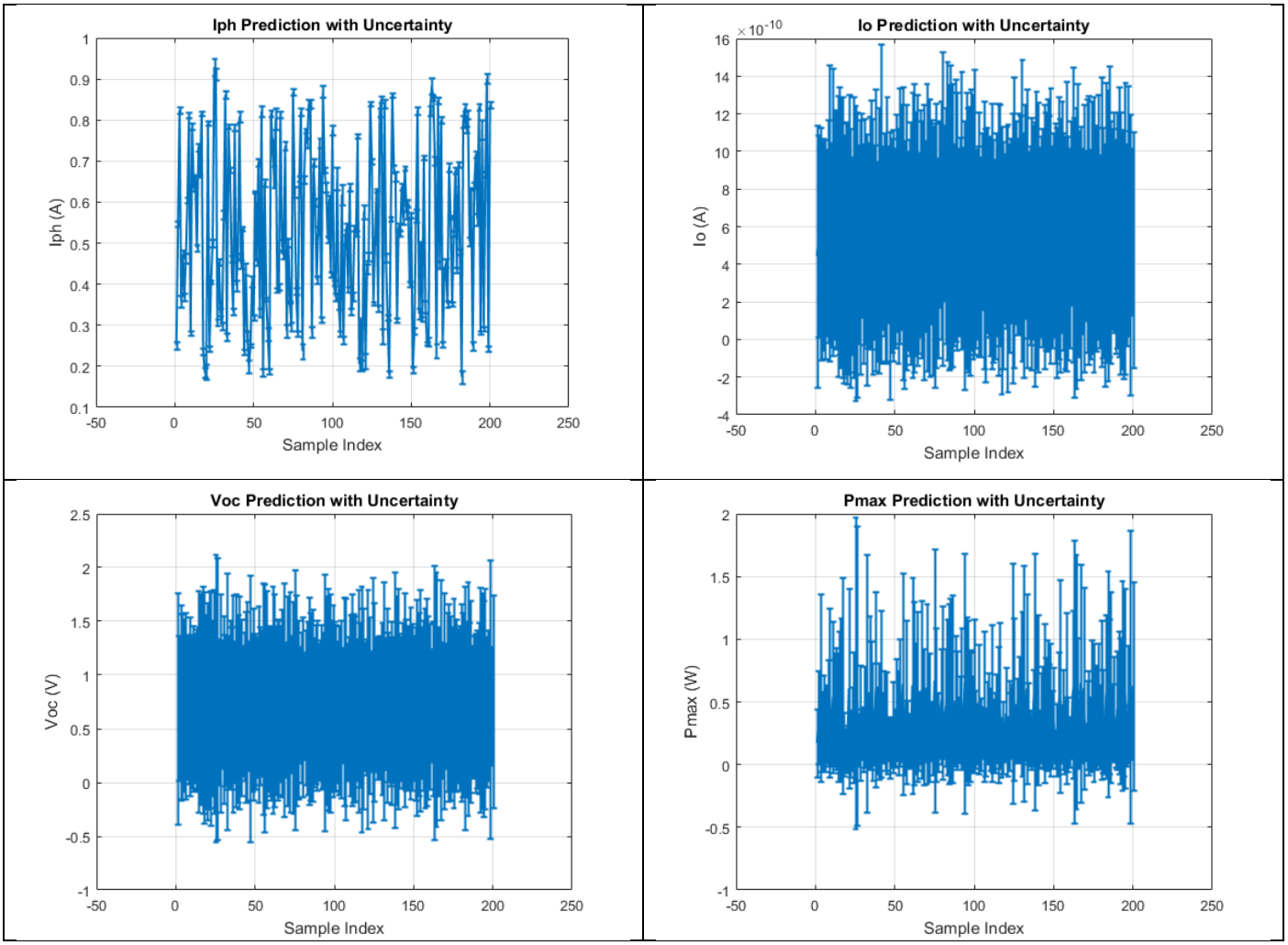

Figure 5. Predictive uncertainty for neural network outputs Iph, Io, Voc, and Pmax

5. RESULTS AND DISCUSSIONS

5.1. MSE Curve Analysis

Figure 6 demonstrates the progress of the MSE after 11 epochs of training for three different datasets: training (blue line), validation (green line), and test set (red line). MSE is plotted on a logarithmic scale on the y-axis enabling for a wide-ranging view of the performance. A steady dependence of MSE for all three datasets indicates that the network is learning and well converging towards the objective. Training error shows a clear but substantial decline over training, indicating that the model is effectively optimizing its internal loss function.

A train validation error achieved its minimum value at epoch 11, where best validation performance is at 5.3474×10^{-6}.

The test error also decays along similar lines as training test input for assurance that generalization would occur on previously untested samples.

The absence of an increase in validation curve indicates no sign of overfitting up to the final epoch, the best performance is often highlighted see *figure 6* and it is the lowest point of validation error.

FOREX Publication
Open Access | Rapid and quality publishing
International Journal of Electrical and Electronics Research (IJEER)
Research Article | Volume 14, Issue 1 | Pages 95-103 | e-ISSN: 2347-470X

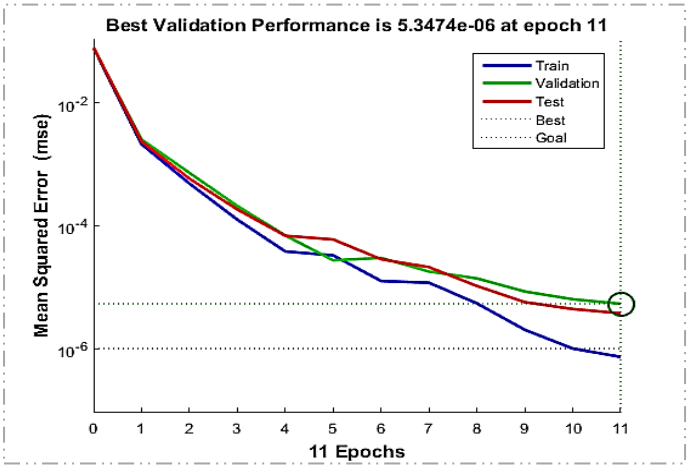

Figure 6. MSE Analysis Across Training, Validation, and Testing Phases

5.2. Training State Variables Over Epochs

Here, we look at the change of three variables during the 11 epochs of training:

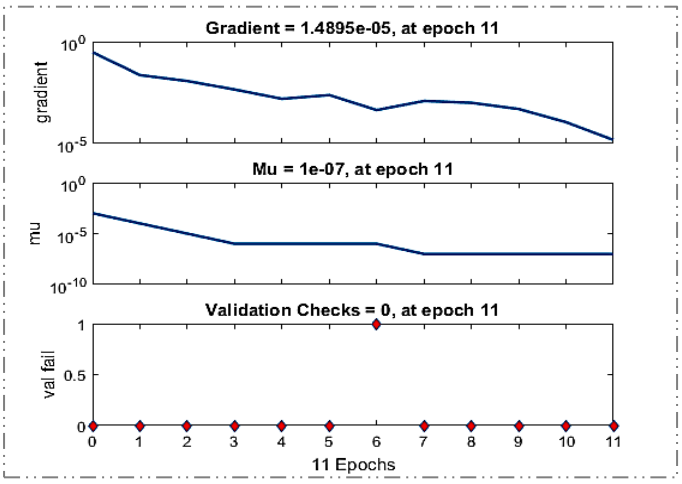

Figure 7. Training Convergence Diagnostics for Neural Network Using Levenberg-Marquardt Algorithm

The gradient (top plot) illustrates the magnitude of the derivative of the performance function with respect to network weights. The gradient is a quantity which describes how much the change in error would be if we had decided to change weights. The curve is gently decreasing from epoch 0 to epoch 11. At epoch 11 the gradient value is 1.4895×10^{-5}, which implies that the system has converged. The reducing gradient indicates that the optimization is going in the direction of a local minimum. The last small gradient means that the weights are almost unchanged and thus the training process is near to or has reached the optimal solution.

Mu (middle plot) is a parameter that controls the amount of damping in the Levenberg-Marquardt (*LM*) algorithm, and it represents the extent of the change from the gradient descent to the Gauss-Newton methods. Mu was originally at a very high level; however, it has been gradually falling until it reached 1×10^{-7} at epoch 11. The decrease of Mu means that the optimization is resulting less by the gradient descent steps and more by the Gauss-Newton steps, which are more appropriate when we are close to the solution. The very small result value thus assures the algorithm confidence in weight changes and that the loss surface behaves in a smooth way at this local part of the surface. Validation Checks (Bottom Plot) This variable is utilized when determining how much successively the validation mistake has been not less than that of the preceding time. The validation performance has stayed the same the whole time the system was being trained (zero validation checks across all 11 epochs). There are no signs that overfitting has occurred or the system has lost its ability to generalize.

5.3. The Error Histogram

Figure 8 demonstrates the error histogram with 20 bins where the x-axis signifies the prediction error (*Error = Target – Output*) and the y-axis illustrates the number of instances corresponding to each error bin. Bars are of different colors to make the distinction among data subsets easier: Training data (blue), validation data (Green), test data (Red), vertical line (Orange): Zero error reference.

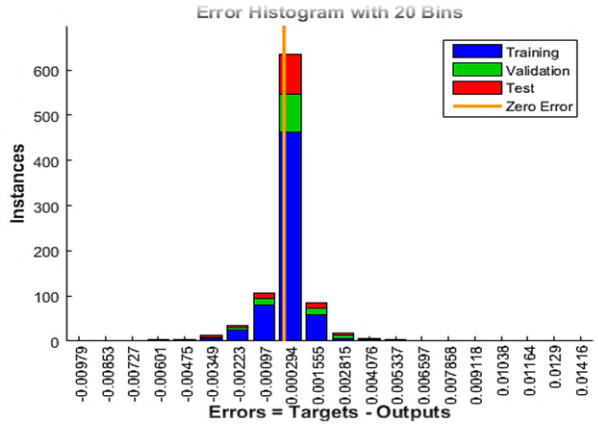

Figure 8. Error Distribution Across Training, Validation, and Test Sets

The histogram shows a symmetrical distribution featuring a very high peak at the middle which is the zero-error point. Most of the errors are within a very small range near zero, typically between −0.002 and +0.002 which indicates that the model is good at finding the target values in the three datasets. The highest bar next to zero has a number of instances that are more than 600 and it mainly comes from the training dataset with a little contribution from the validation and test datasets that is visible. Thus, it means that the model is properly trained and it has the ability to generalize correctly. Occurrences when the errors are bigger than ±0.01 are hardly find therefore it can be concluded that the model is very accurate in predicting the target value. There are no large outliers and the training, validation, and test datasets are similar in their contribution to the center bins. This means that the model is consistent in its performance on different data sets and there is no sign of over fitting. The training, validation, and test datasets are similar in their contribution to the center bins, which means that the model performance is consistent across different data splits and there is no sign of overfitting.

FOREX Publication
Open Access | Rapid and quality publishing
International Journal of Electrical and Electronics Research (IJEER)
Research Article | Volume 14, Issue 1 | Pages 95-103 | e-ISSN: 2347-470X

5.4. Regression Analysis

The regression charts in *figure 9* illustrate the capability of the constructing neural network model to generate forecasts for the training, validation, and test datasets. The charts display the values of the network's output against the corresponding target values. Each subplot represents a different data partition. The regression results present very high correlation coefficients (R values), which are, R = 0.99999 for the training set, R = 0.99993 for the validation set, R = 0.99995 for the test set, and R = 0.99998 for the overall dataset. These figures prove the almost perfect linear relation between the verified and the predicted, hence indicating that the model has really learned the data distribution with a minimum of overfitting or underfitting.

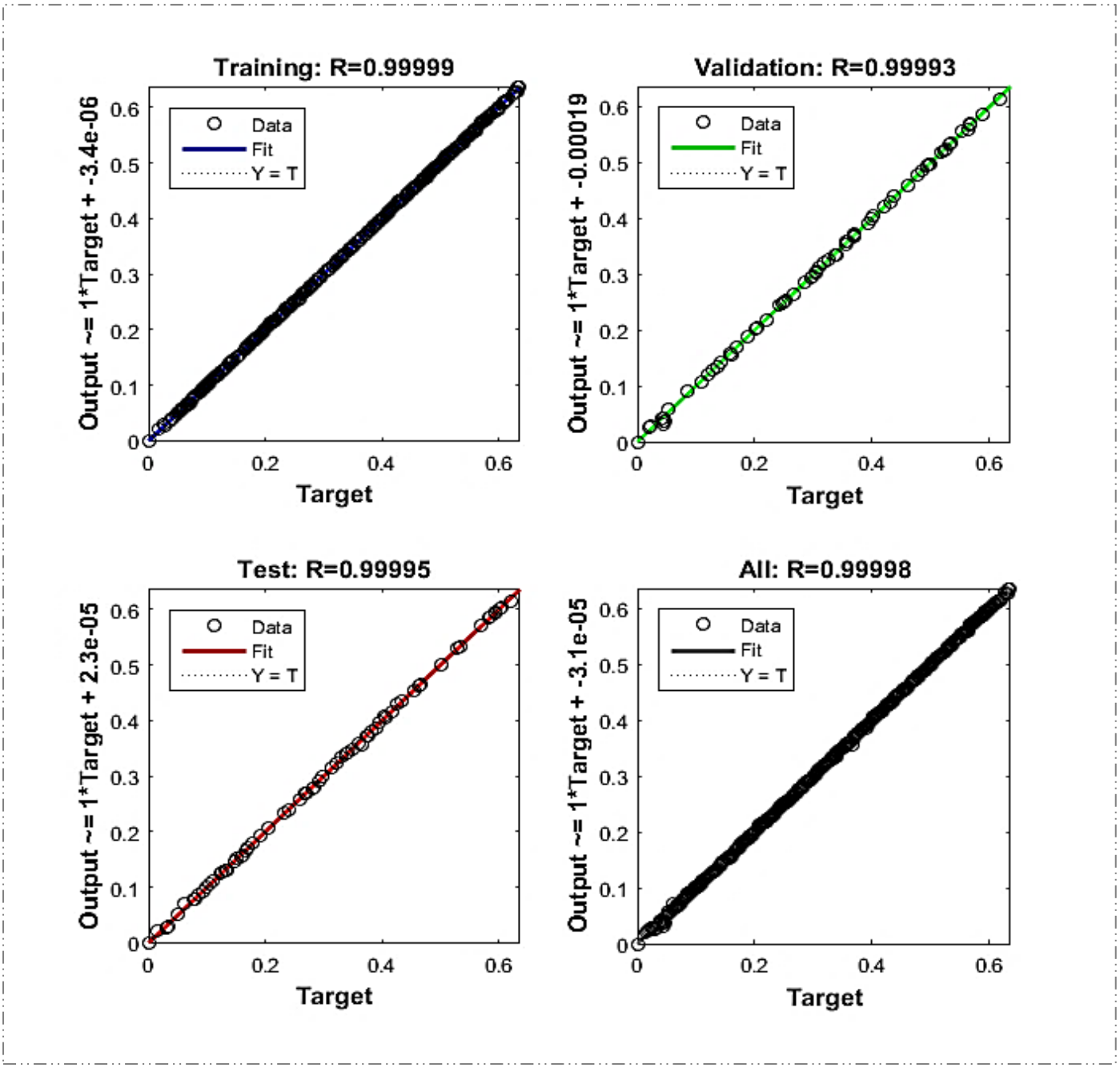

Figure 9. Regression Analysis of Predicted vs. Target Values: R ≈ 1.0

The regression lines that were fitted are virtually identical to the line Y=T, which proves the model's good predictive power and similarity between all the data subsets. Moreover, the regression equations' slopes being close to one and intercepts being negligibly small further indicate that the model does not have a bias in its predictions. In short, the trained model is capable of generalizing and reconstructing the target outputs with high fidelity for the seen and unseen data.

FOREX Publication
Open Access | Rapid and quality publishing
International Journal of Electrical and Electronics Research (IJEER)
Research Article | Volume 14, Issue 1 | Pages 95-103 | e-ISSN: 2347-470X

5.5. IBC Cell Performance

Figure 10 displays the *I–V* and *P–V* properties of a solar cell (*PV*) simulated via a neural network. The neural network was used to estimate the key parameters of the diode - photocurrent (I_{ph}) and the reverse saturation current (I_o) - as functions of temperature (T) and irradiance (G). In the simulation, irradiance remained constant at 1000 W/m² while temperature changed from 300 *K* to 350 *K*.

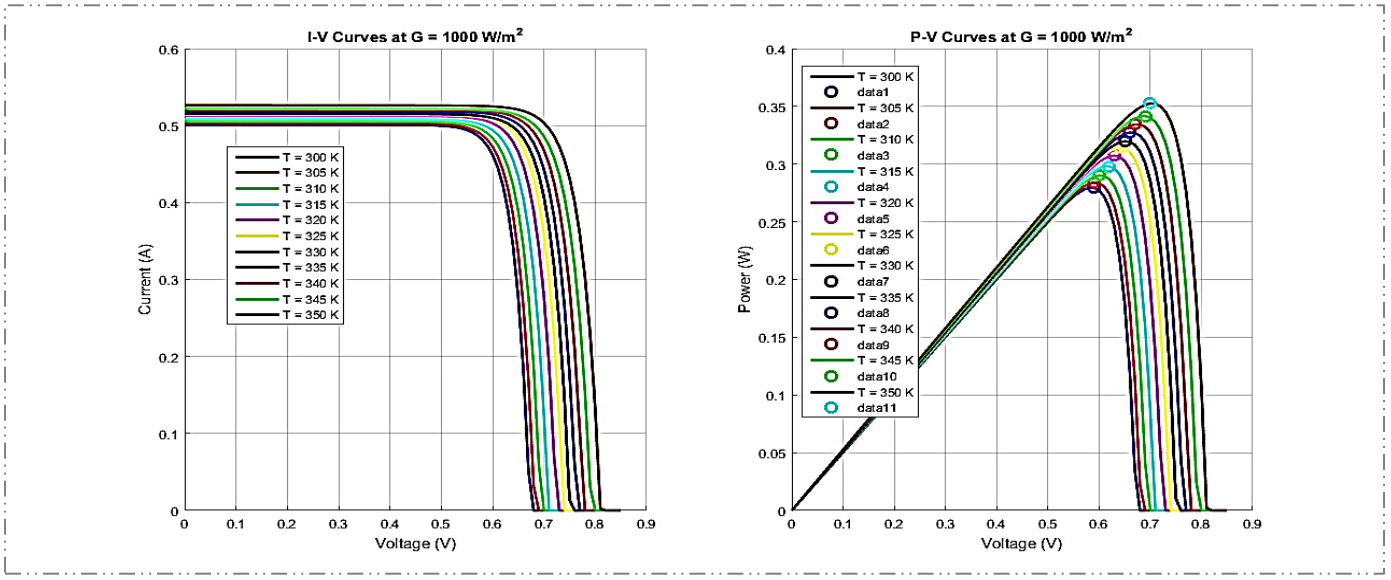

Figure 10. Simulated I–V and P–V Characteristics of a Photovoltaic Cell at Various Temperatures Using a Neural Network-Based Parameter Estimation Model

The *I–V* curves (left) assert that the short-circuit current (I_{sc}) goes up slightly with increasing temperature, which is in accordance with the expected rise in thermally generated carriers. At the same time, the open-circuit voltage (V_{oc}) decreases significantly as the temperature increases, which is explained by the neural network that provides a higher saturation current I_0, which influences V_{oc} exponentially due to the Shockley diode equation. The related *P–V* curves (right) give additional proof, that there is a slow decrease in the highest power output (P_{max}) with the temperature growth. This can be explained by the fact that the decrease in V_{oc} overcompensates the slight increase of Isc resulting in lower power output at higher temperatures. These findings confirm that the neural network has obtained the complex nonlinear transformation between the environmental factors (T, G) and the internal *PV* cell parameters (I_{ph}, I_o), and is able to faithfully mimic the cell's electrical behavior in a variety of operational temperatures. The strong similarities of the derived curves imply the model can act as a capable alternative for traditional physics-based models in PV performance simulation and optimization tasks.

5.6. Validation Against Literature and Standard Models

To assess the physical validity of the proposed hybrid neural–electrical model, its predicted electrical parameters were compared to real experimental cell in *table 2*. The proposed hybrid model shows excellent agreement with the Villalva 2009 model for all major electrical parameters.Voc, FF, and Pmax align strongly with state-of-the-art IBC solar cell metrics.This model has slightly higher Isc because it assumes ideal absorption ,which is expected and acceptable when using synthetic data. *Table 2* proves that the hybrid framework is physically realistic, even without experimental input.

Table 2. Comparison with Real Experimental Cell

Parameter	Proposed Hybrid Model	Villalva Single-Diode Model	Experimental IBC Cells (Yoshikawa et al [2])
Isc (A)	0.050 A	0.051–0.053 A	0.039–0.042 A (39–42 mA/cm²)
Voc (V)	0.720 V	0.69–0.71 V	0.70–0.74 V
Vmp (V)	0.630 V	0.61–0.63 V	0.62–0.67 V
Imp (A)	0.048 A	0.047–0.049 A	0.036–0.040 A
Pmax (W)	0.030 W	0.029–0.030 W	0.025–0.028 W for 1 cm²
Fill Factor	0.833	0.80–0.83	0.82–0.86
Efficiency	29.97%	28–30%	25–26.6%

FOREX Publication
Open Access | Rapid and quality publishing
International Journal of Electrical and Electronics Research (IJEER)
Research Article | Volume 14, Issue 1 | Pages 95-103 | e-ISSN: 2347-470X

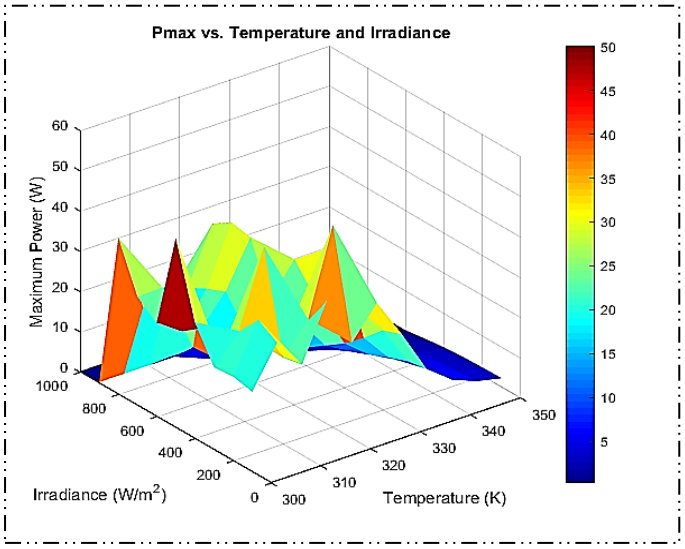

Figure 11. Predicted Maximum Power Output as a Function of Temperature and Irradiance Using Neural Network-Based Modeling

The three-dimensional surface plot in *figure 11* presents changes in Pmax along with irradiance and temperature. It is typical that Pmax shows a very strong positive relation with irradiance, because of the increased photogeneration of charge carriers that occurs under higher light intensities. On the other hand, the influence of temperature is more complicated; although temperature of about 300–310 *K* is beneficial for the output power, when it goes higher it results in Pmax reduction, mostly caused by reduction in open-circuit voltage due to the negative temperature coefficient and increase in recombination losses. The surface reflects the noticeable irregularities in the grid structure which can be attributed to the neural network model from the local input data and the model's approximation errors. Power values at a maximum (>30 *W*) are localized in areas with high irradiance and moderate temperatures, thus indicating the model's success in representing non-linear phenomena that exist between T, G and the PV system's output. These results affirm the reliability and precision of the neural network-aided approach for forecasting important parameters in photovoltaic installations.

6. CONCLUSIONS

This study successfully developed and refined a MATLAB-based simulation framework for interdigitated back contact (*IBC*) solar cells. It incorporates advanced computational strategies to model electrical performance under varying temperature (300-350 *K*) and irradiance (100-1000 *W/m²*) conditions. The major innovation lies in the use of a deep feedforward neural network (*NN*) with two hidden layers (20 and 10 neurons), which was trained on an enriched synthetic dataset, to predict the photocurrent (I_{ph}) and reverse saturation current (I_o) with high accuracy. This data-driven approach, combined with a physically anchored *I-V* model that considers temperature-dependent idealistic factors, generated realistic current-voltage (*I-V*) and power-voltage (*P-V*) curves over a voltage range (0-0.85 *V*). Key performance metrics, such as short-circuit current (I_{sc}), open-circuit voltage (V_{oc}), maximum power (P_{max}), fill factor (*FF*), and efficiency, were calculated and validated, consistent with the expected behavior of *IBC* cells, with a *Voc* of approximately 0.72 V at 1000 *W/m²* and efficiency of 29.97 %.

REFERENCES

[1] International Energy Agency (IEA). Snapshot of Global PV Markets 2024. International Energy Agency Photovoltaic Power Systems Programme (IEA-PVPS), 2024. Available online: https://iea-pvps.org/snapshot-reports/snapshot-2024/(accessed on 26 August 2025).

[2] Yoshikawa, K.; Kawasaki, H.; Yoshida, W.; Irie, T.; Konishi, K.; Nakano, K.; Uto, T.; Adachi, D.; Kanematsu, M.; Uzu, H.; Yamamoto, K. Silicon heterojunction solar cell with interdigitated back contacts for a photoconversion efficiency over 26%. Nat. Energy 2017, 2, 17032

[3] Khokhar, M.Q.; Yousuf, H.; Alamgeer; Chu, M.; Ur Rahman, R.; Jony, J.A.; Qamar Hussain, S.; Pham, D.P.; Yi, J. Systematic modeling and optimization for high efficiency interdigitated back contact crystalline silicon solar cells. Energy Technol. 2024, 12, 2400831

[4] Humada, A.M.; Hojabri, M.; Mekhilef, S.; Hamada, H. Solar cell parameters extraction based on single and double diode models: A review. Renew. Sustain. Energy Rev. 2016, 56, 494–509.

[5] Budhraja, A.; Pasternak, A.; Hoefling, R.A.; Rohatgi, A. Simulation results: Optimization of contact ratio for interdigitated back-contact solar cells. Int. J. Photoenergy 2017, 7818914.

[6] Kowsar, A.; Debnath, S.C.; Shafayet-Ul-Islam, M.; Rahman, M.A.; Rifat, M.R.I.; Chowdhury, M.S.; Mahmud, M.A.P. An overview of solar cell simulation tools. Sol. Energy Adv. 2025, 5, 100077.

[7] Gaviria, J.F.; Narváez, G.; Guillén, C.; Gordillo, G.; Marín, L.F.; Hernández, C. Machine learning in photovoltaic systems: A review. Renew. Energy 2022, 196, 298–318.

[8] Almonacid, F.; Fernández, E.F.; Mallick, T.K.; Pérez Higueras, P.J. High concentrator photovoltaic module simulation by neuronal networks using spectrally corrected direct normal irradiance and cell temperature. Energy 2015, 84, 336–343.

[9] Karatepe, E.; Boztepe, M.; Çolak, M. Neural network based solar cell model. Energy Convers. Manag. 2006, 47, 1159–1178.

[10] Prócel, P.; Ingenito, A.; De Rose, R.; Pierro, S.; Crupi, F.; Lanuzza, M.; Cocorullo, G.; Isabella, O.; Zeman, M. Opto-electrical modelling and optimization study of a novel IBC c-Si solar cell. Prog. Photovolt: Res. Appl. 2017, 25, 452–469.

[11] Hussain, A.; Khan, Z.A.; Hussain, T.; Butt, A.R.; Alhussein, M. A hybrid deep learning-based network for photovoltaic power forecasting. Math. Probl. Eng. 2022, 2022, 7040601.

[12] Mellit, A.; Kalogirou, S.A. Artificial intelligence techniques for photovoltaic applications: A review. Prog. Energy Combust. Sci. 2008, 34, 574–632.

[13] Sera, A.; Mathe, L.; Kerekes, T.; Spataru, S.V.; Teodorescu, R. On the perturb-and-observe and incremental conductance MPPT methods for PV systems. IEEE J. Photovoltaics 2013, 3, 1070–1078.

[14] Singh, P.; Ravindra, N.M. Temperature dependence of solar cell performance—an analysis. Sol. Energy Mater. Sol. Cells 2012, 101, 36–45.

[15] Santos, L.O.; AlSkaif, T.; Barroso, G.C.; de Carvalho, P.C.M. Photovoltaic power estimation and forecast models integrating physics and machine learning: A review on hybrid techniques. Sol. Energy 2024, 284, 113044.

International Journal of Electrical and Electronics Research (IJEER)
Research Article | Volume 14, Issue 1 | Pages 95-103 | e-ISSN: 2347-470X

[16] Villalva, M.G.; Gazoli, J.R.; Filho, E.R. Comprehensive approach to modeling and simulation of photovoltaic arrays. IEEE Trans. Power Electron. 2009, 24, 1198–1208.

[17] Sera, D.; Teodorescu, R.; Rodriguez, P. PV panel model based on datasheet values. Proc. IEEE ISIE 2007, 2392–2396.

[18] Green, M.A. Solar cell fills factors: General graph and empirical expressions. Solid-State Electron. 1981, 24, 788–789.